Excitatory cholecystokinin neurons in CA3 area regulate the navigation learning and neuroplasticity

Fengwen Huang[1,2*], Abdul Baset[2], Stephen Temitayo Bello[2]

[1]Department of Neuroscience, City University of Hong Kong, Kowloon Tong, Hong Kong, P.R. China

[2]Department of Ophthalmology, Stanford University School of Medicine, Palo Alto, CA, USA.

[*]Corresponding author:
fwhuang2@stanford.edu (F.W. Huang).

Abstract

Hippocampus, a key hub of neural circuits for spatial learning and memory, has attracted tremendous studies. Neuronal information processing in the hippocampus can be regulated by many types of neuropeptides. Cholecystokinin (CCK), the most abundant neuropeptide in the central nervous system which is involved in modulating neuronal functions, such as cognition, memory and neuroplasticity, is widely expressed in the hippocampus. However, whether local excitatory CCK neurons modulates hippocampal function is still unclear. In this study, we showed that CA1 pyramidal neurons receive projections from excitatory CCK neurons in area CA3 ($CA3^{CCK}$ neurons). Subsequently, activation of the CA1-projecting $CA3^{CCK}$ neurons triggers the release of CCK. Then, we found that activity of $CA3^{CCK}$-CA1 neurons supports the hippocampal-dependent tasks. Furthermore, inhibition of $CA3^{CCK}$-CA1 projections or knockdown of $CA3^{CCK}$ gene expression markedly impaired the behavioral tasks and neuroplasticity. Taken together, these results may add to a better understanding of how neuromodulators regulate the neural functions in central nervous system.

Key words: hippocampus; cholecystokinin; long-term potentiation; neuropeptide.

Introduction

Neuropeptides are expressed and secreted throughout the mammalian brain where they play key roles in modulating neuronal activities and behaviors (Swaab 1982; Merighi et al., 2011; De Wied 1997). Long-term potentiation (LTP) and long-term depression (LTD) have been considered cellular

mechanisms correlated with learning and memory in the central nervous system (CNS) (Grasselli and Hansel 2014). Hippocampus is a unique brain region that is critically involved in learning and memory (Ranganath and Hsieh 2016), and how neuromodulations affect the function of the hippocampal system has attracted lots of interest (Gedankien et al., 2023; Broussard et al., 2016; Li and Gao 2016; Karayol et al., 2021).

During the past decades, many studies have identified the neuronal mechanisms that guide neuropeptides across the hippocampal function and examined whether neuropeptides undergo specific adaptations in response to external innervation. However, most investigations focus on the classical monoamine neuromodulators, including acetylcholine (Ach), dopamine (DP), norepinephrine (NE), serotonin (ST), etc (Gedankien et al., 2023; Broussard et al., 2016; Li and Gao 2016; Karayol et al., 2021). Ach can regulate neuronal excitability and synaptic transmission in the mammalian brain (Takács et al., 2018). Several studies have demonstrated that stress increases Ach release in a brain region-specific manner (Picciotto et al., 2012; Mineur et al., 2013). For example, stress-induced increase in Ach level in the rat hippocampus and cortical area. DP is a critical modulator in neuronal circuitry, which has been shown to be involved in a variety of behavioral phenomena in the hippocampus, such as episodic memory formation (Chowdhury et al., 2012), spatial learning (Kempadoo et al., 2016), and synaptic plasticity (Hamilton et al., 2010). DP innervation from the midbrain is mainly via the dopamine receptor (D1/D5) when it is released into the dorsal hippocampus (Cai and Ford 2018). Additionally, the role of NE in memory retrieval requires signaling through the β1-adrenergic receptor in the hippocampus (Chang et al., 2011). The hippocampus has one of the denser inputs of adrenergic terminals (containing NE) in the CNS, indicating that the adrenergic system plays a role in learning and memory (Goodman et al., 2021). Interestingly, high concentration of serotoninergic fibers in the forebrain is in stratum lacunosum-moleculare (SLM) of hippocampal areas CA1 and CA3, where the axons of layer III neurons in the entorhinal cortex form excitatory synapses with the distal apical dendrites of pyramidal cells (Cai et al., 2013). This temporoammonic pathway is required for some spatial recognition tasks and for long-term consolidation of spatial memory. All these studies implied that neuropeptides play a critical role in the hippocampal system and influence subsequent behaviors.

Cholecystokinin (CCK), one of the most abundant neuropeptides in the CNS (Ma and Giardino 2022),

has not received much attention and its function in the hippocampal system has been generally underestimated. Although several reports have shown that CCK enhances the excitatory synaptic transmission in the hippocampus and improves learning performance (Wei et al., 2013; Reisi et al., 2015). However, the exact mechanism by which CCK regulates the hippocampus plasticity and hippocampus-dependent behaviors has not yet been fully elucidated. To address this knowledge gap, we adopted the transgenic mice, optogenetics, GPCR-based sensor, extracellular recording, chemogenetics, RNA interference technique, calcium recording and behavioral task to investigate: 1) the distribution profile of CCK-positive neurons in the CA3 area of dorsal hippocampus (DHP), 2) activation of $CA3^{CCK}$ neurons secrets the CCK at hippocampal SC-CA1 synapses. 3) the causal relationship between the Ca^{2+} response of excitatory $CA3^{CCK}$ neurons and hippocampal functions. This study should bring conceptual advances to the foundation of neuropeptide modulation and the studies of hippocampus-dependent learning and memory.

Results

Distribution profile of CCK-positive neurons in the DHP

Although many studies have well documented the role of inhibitory CCK in the hippocampus (Klausberger et al., 2005; Ali 2007; Hefft and Jonas 2005), the function of excitatory CCK in the hippocampus is still unclear. To address this issue, we developed the transgenic CCK Cre::Ai14 (Tdtomato) reporter mice that express the red fluorescent protein tdTomato upon Cre-mediated recombination. This mouse line is suited in examining the distribution profile of CCK positive neurons in the dorsal hippocampus (DHP) (**Figure 1A-B**). Interestingly, we found that the proportion of CCK positive neurons in area CA1 and CA3 of CCK Cre/Ai14 mice was around 8.50 % and 20.34 %, respectively (**Figure 1C-D**). We further examined the properties of these CCK neurons in areas CA3, which may send dense CCK^{+} projections to the area CA1. Interestingly, excitatory neuronal marker CamkIIα was intensively colocalized with Tdtomato expressing CCK neurons in the area CA3 (**Figure 1E**). Moreover. the CCK proteins also show high co-localization in excitatory neurons in CA3 area (**Figure 1F**).

Furthermore, to validate the projection of CA1-projecting $CA3^{CCK}$ neurons in the DHP, we injected the Cre-dependent retrograde axonal transport of AAV (Retro-AAV-EF1α-DIO-EYFP) into the area CA1 (**Figure 1G**). Unsurprisingly, CA3 neurons were widely labelled with green fluorescent protein (GFP;

Figure 1H). Moreover, high degree of colocalization between CamKIIα marker and GFP was observed in the area CA3 (**Figure 1I-J**; 90.15± 15 %). These anatomy results suggest that excitatory CA3 neurons are densely expressed and may exerts neuronal functions in central nervous system.

Excitatory CA3 neurons can secret the neuropeptide CCK

Next, to investigate the neurotransmission property of the excitatory CCK neurons in CA3 area ($CA3^{CCK}$), we utilized the Cre-dependent excitatory AAV (AAV9-DIO-CamKIIα-ChrimsonR-mCherry) to specifically target the excitatory $CA3^{CCK}$ neurons in CCK-Cre mice (**Figure 2A**). Four weeks after the AAV injection and expression in *vivo*, robust expression of ChrimsonR-mCherry was observed in $CA3^{CCK}$ neurons (**Figure 2B-C**). Subsequently, we used the 636 nm wavelength light to activate and elicit the field excitatory post synaptic potentials (L-fEPSPs) in ChrimsonR-mCherry expressing brain section (**Figure 2D**). Intriguingly, we noticed that the L- fEPSPs were almost completely blocked by the AMPA receptor antagonist (CNQX; 20 μM) and NMDA receptor antagonist (APV; 100 μM) in the area CA1, suggesting an excitatory nature of CA1-projecting $CA3^{CCK}$ pathway (**Figure 2E-F**).

To determine whether the neuropeptide CCK can be secreted from the CA3 derived excitatory CA3-CA1 projections, we adopted the GPCR-based CCK-BR sensor to monitor the release of CCK from the CA3-CA1 terminals in CA1 area under the external light stimulation (**Figure 2G**). To achieve this goal, AAV9-DIO-CamKIα-ChrimsonR-mCherry and AAV9-hSyn-CCK-GFP-2.3 (AAV9-hSyn-GFP as control) were injected into the CA3 and CA1 area to target the CA3-CA1 projection and CA1 pyramidal neurons (CA1 PNs) in CCK-Cre mice (**Figure 2H**). Subsequently, stimulation fiber and recording fiber were implanted upon the CA3 and CA1 area. Four weeks after the AAVs injection and expression (**Figure 2I-J**), high-frequency theta burst light stimulation (L-TBS) was delivered to the simulation fiber (**Figure 2K**), which mimic the neural rhythm in hippocampus in *vivo*. Interestingly, transient increase in CCK sensor was monitored by L-TBS of ChrimsonR-expressing $CA3^{CCK}$ neurons, while no significant amplification was found in control (**Figure 2L-N**; Two samples T-Test, $t = 3.79$ $df = 10$, $p = 0.004$). These results indicates that neuropeptide CCK can be secreted from the excitatory $CA3^{CCK}$ neurons under the mimic physiological conditions.

$CA3^{CCK}$ neurons fire actively during hippocampal-dependent tasks

We next wonder about the activity status of $CA3^{CCK}$ neurons during hippocampal-dependent tasks (**Figure 3A)**. Thus, we injected the AAV9-CamkIIα-DIO-GCaMP6s into the area CA3 of CCK Cre

mice to monitor the calcium-response of $CA3^{CCK}$ neurons during the behavioral task (**Figure 3B**). In novel object location (NOL) task, mice spent comparable time on object exploration between object 1 (O1) and object 2 (O2) in the training phase, while mice spent significantly more time on interacting with object in the novel place (O2") compared with the object in the familiar site (**Figure 3C**; two way mixed ANOVA, Bonferroni adjustment; $F_{1,10} = 4.58$, $p = 0.05$; Training: O1 11.42 ± 1.56 s v.s. O2 10.62 ± 2.18 s, $p = 0.73$; Testing: O1 8.62 ± 0.99 s v.s. O2": 13.95 ± 1.60 s, $p = 0.02$). Concurrently, we examined the Ca^{2+} responses of excitatory $CA3^{CCK}$ neurons during object exploration. Interestingly, we observed that object exploration elicited a significant increase in fluorescence intensity in both training phase and testing phase (**Figure 3D-E**). Moreover, Ca^{2+}signal of $CA3^{CCK}$ neurons elicited by novel locations also show significant difference compared with familiar locations (**Figure 3F**; two way mixed ANOVA, Bonferrori adjustment; $F_{1,10} = 1.88$, $p = 0.20$; Training ($\Delta F/F$): O1 0.27 ± 0.07 % v.s. O2 0.31 ± 0.08 %, $p = 0.91$; Testing ($\Delta F/F$): O1 0.27 ± 0.09 % v.s. O2" 0.41 ± 0.12 %, $p = 0.04$), which implies that excitatory $CA3^{CCK}$ neurons are critical for specific spatial memory and learning.

Furthermore, we examined whether the excitatory $CA3^{CCK}$ neurons are necessary for performing the MWM paradigm (**Figure 3G**). Intriguingly, in the naive training (trial 1), a robust and persistent Ca^{2+} responses were observed during the initial learning (**Figure 3H and Figure 3I**). Nevertheless, after the completion of training, $CA3^{CCK}$ neurons produced a relatively smaller Ca^{2+} signal on the training day 3 with an averaged escape latency of < 10 s to locate the hidden platform (**Figure 3H and Figure 3J**; **Figure 3K**: Paired sample t-test, df = 5, t = 2.80; Trial 1: 1.32 ± 0.74 % v.s. Trial 9: 0.75 ± 0.35 %, $p = 0.038$), this result further supports the conclusion that excitatory $CA3^{CCK}$ neurons plays a direct role in the animals' accurate spatial learning and memory formation.

Chemogenetic inhibition of the excitatory $CA3^{CCK}$-CA1 pathway impairs behavioral tasks

Next, to further confirm the necessity of excitatory $CA3^{CCK}$-CA1 pathway for performance of the hippocampal-dependent behaviors. We adopted the chemogenetic approach, which is a powerful technique for specific disturbance of neuronal activity through virus-mediated DREADD expression in combination with its agonist clozapine N-oxide (CNO) (Gomez et al., 2017), to specifically target the excitatory $CA3^{CCK}$ neurons. Firstly, we injected the Cre dependent AAV expressing the inhibitory DREADD (hM4DGi) to infect the excitatory $CA3^{CCK}$ neurons and AAV carrying mCherry as control (**Figure 4A**) and implanted the drug cannular upon the CA1 area. Four weeks after the AAV injection

and expression (**Figure 4B**), we conducted the MWM task in the two groups of mice to assess the role of CA1-projecting $CA3^{CCK}$ neurons in hippocampus-dependent spatial learning (**Figure 4C**). Thus, we delivered the CNO (300 nl; 10 μM) via the cannulas to inhibit CCK^{+} CA3-CA1 projections upon the area CA1 before conducting the MWM. Then, two groups of mice were subjected to the visible platform task to evaluate their swimming capability. Both groups of mice displayed comparable swimming speed and the speed time in finding the visible platform (**Figure 4D**; two sample t-test, df = 18, t = 0.22, HM4D(Gi): 24.3 ± 1.66 cm/s v.s. mCherry: 23.8 ± 1.52 cm/s, p = 0.83. **Figure 4E**; two sample t-test, df = 18, t = 1.09, HM4D(Gi): 30.86 ± 2.587 s v.s. mCherry: 34.21 ± 2.12 s, p = 0.29). During the hidden platform task, the mice only expressing mCherry gradually spent less time in locating the platform compared to the mice infected with hM4D(Gi) (**Figure 4F**; two-way mixed ANOVA, Bonferroni adjustment; $F_{4,15} = 1.24$, p = 0.34; HM4D(Gi): 24.18 ± 4.36 s v.s. mCherry: 15.12 ± 2.13 s on day 5, p = 0.003). Additionally, the control mice showed higher percentage on the target quadrant on the memory retention day, while lower percentage of the occupancy in experimental mice (**Figure 4G-H**; two-way mixed ANOVA, Bonferroni adjustment; $F_{3,16} = 1.19$, p = 0.34; HM4D(Gi): 27.91 ± 2.75 % v.s. mCherry: 42.31 ± 3.82 % in quadrant 3, p = 0.02). These results demonstrated that excitatory $CA3^{CCK}$-CA1 pathway is required for animals to perform adequately in spatial learning.

In the NOL task (**Figure 4I**), both groups of mice showed equal motivation to explore objects (**Figure 4J**; two sample t-test, df = 18, t = -0.31, hM4D(Gi): 81.18 ± 9.14 s v.s. mCherry: 85.35 ± 9.67 s, p = 0.76). Compared with the control mice, the experimental group was unable to distinguish the novel and familiar object location in the test phase, and presented low discrimination ratio (**Figure 4K**; two-way mixed ANOVA, Bonferroni adjustment; $F_{1,18} = 4.58$, p = 0.04; hM4D(Gi): Familiar 40.83 ± 5.27 s v.s. Novel: 43.46 ± 7.40 s, p = 0.66; mCherry 34.38 ± 3.58 s v.s. Novel: 55.35 ± 6.11 s, p = 0.003. **Figure 4L**; two sample t-test, df = 18, t = 0.77, hM4D(Gi): -0.003 ± 0.09 v.s. mCherry: 0.22 ± 0.06, p = 0.03), indicating suppression of excitatory $CA3^{CCK}$-CA1 pathways impaired the spatial memory. Taken together, we can conclude that excitatory $CA3^{CCK}$ neuron is an essential and functional component in the hippocampal system.

Chemogenetic inhibition of the excitatory $CA3^{CCK}$-CA1 pathway attenuates LTP formation

Since the LTP in the hippocampus is commonly considered a key cellular mechanism that underlies spatial learning and memory (Ge et al., 2010). To confirm whether excitatory $CA3^{CCK}$-CA1 pathway are directly involved in LTP formation, we further conducted the electrophysiological recording in *vitro*. Four weeks after the AAV injection and expression (**Figure 5A-B**), hippocampal slices were subjected to electrophysiological recording to test the effect of CNO on the neuroplasticity of excitatory $CA3^{CCK}$-CA1 pathway (**Figure 5C**).

After the baseline recording, the slope of fEPSPs decreased gradually with the CNO treatment while no significant changes were observed in controls (**Figure 5D-E**; two-way mixed ANOVA, Bonferroni adjustment; $F_{1,13} = 78.32$, $p < 0.001$; hM4D(Gi): Pre_{ex} 100.42 ± 0.18 % v.s. $Post_{ex}$ 78.07 ± 1. 52 %, $p < 0.001$; mCherry: Pre_{ctrl} 100.15 ± 0.48 % v.s. $Post_{ctrl}$ 98.90 ± 2.90 %, $p = 0.60$, $Post_{ex}$ v.s. $Post_{ctrl}$, $p < 0.001$), indicating that neuronal activities of the excitatory CA1-projecting $CA3^{CCK}$ neurons were remarkably suppressed. Then, we further employed the E-TBS protocol for the LTP induction under this condition (**Figure 5F**). Intriguingly, the extent of LTP formation in the slices expressing hM4D(Gi) was significantly smaller than those in the control group (**Figure 5G-H**; two way mixed ANOVA, Bonferrori adjustment; $F_{1,13} = 9.46$, $p = 0.01$; HM4D(Gi): Pre_{ex} 99.65 ± 0.31 % v.s. $Post_{ex}$ 111.52 ± 2.40 %, $p < 0.001$, mCherry: Pre_{ctrl} 100.41 ± 0.29 % v.s. $Post_{ctrl}$ 125.17 ± 3.43 %, $p = 0.001$, $Post_{ex}$ v.s. $Post_{ctrl}$, $p = 0.005$), hinting that $CA3^{CCK}$ neurons are involved in the maintenance of hippocampal neuroplasticity.

RNA interference of excitatory $CA3^{CCK}$ expression impairs hippocampal functions

Next, to verify whether neuropeptide CCK in excitatory $CA3^{CCK}$ neurons are also involved in spatial learning and memory, RNA interference (RNAi) strategy was utilized to downregulate CCK expression in $CA3^{CCK}$ neurons (**Figure 6A**). We thus injected AAV9-CamkIIα-DIO-mCherry-shRNA (CCK) into area CA3 to knockdown target gene and AAV9-CamkIIα-DIO-mCherry-shRNA (Scramble) as control. The experimental group was Cre on anti-CCK to knock down the expression of CCK in the area CA3 of CCK Cre mice, while the control group was Cre on anti-scramble. We confirmed the expression of shRNAs in the hippocampus at 4 weeks after AAV injection (**Figure 6B**). Moreover, we further verified that anti-CCK shRNAs faithfully downregulated CCK mRNA levels *in vivo* by using the qPCR technique (**Figures 6C**; two sample t-test, df = 10, t = 4.95, anti-scramble 100 ± 7.03 % v.s. anti-CCK 58.73 ± 7.23 %, P = 0.001). Subsequently, we conducted the MWM task in the two groups of mice to

assess the role of CA1-projecting $CA3^{CCK}$ neurons in the hippocampus-dependent spatial learning (**Figure 6D**).

The two groups of mice injected with anti-CCK and anti-scramble showed comparable swimming speed (**Figure 6E**; two sample t-test, df = 18, t = -0.40, anti-CCK: 23.3 ± 2.75 cm/s v.s. anti-scramble: 24.1 ± 1.41cm/ s, p = 0.69) and swimming time in locating the visible platform above the water surface of the swimming pool (**Figure 6F**; two sample t-test, df = 18, t = -0.51, anti-CCK: 33.4 ± 2.21 s v.s. anti-scramble: 34.9 ± 1.93 s, p = 0.62). Then, mice infected with the anti-CCK showed deficits in spatial learning during the 5 days training (**Figure 6G**; two way mixed ANOVA, Bonferrori adjustment; $F_{4,15}$ = 0.30, p = 0.88; anti-CCK 25.48 ± 2.12 s v.s. anti-scramble 18.05 ± 3.10 s on day 5, p = 0.007), and also exhibited deficiency in memory retention (**Figure 6H-I**; two way mixed ANOVA, Bonferrori adjustment; $F_{3,16}$ = 1.20, p = 0.34; anti-CCK 28.38 ± 1.78 % v.s. anti-scramble 35.76 ± 3.68 % in quadrant 3, p = 0.03). These results suggest that knockdown of CCK expression in area CA3 attenuates spatial learning ability.

In another spatial learning protocol, the novel object location (NOL) task (**Figure 6J**), two groups of mice exhibited equal motivation to explore objects (**Figure 6K**; two sample t-test, df = 18, t = 0.28, anti-CCK: 83.82 ± 5.85 s v.s. anti-scramble: 81.22 ± 7.25 s, p = 0.78). Compared with the control mice (anti-scramble), the mice infected with anti-CCK failed to distinguish between the novel and familiar object location in the test phase, and displayed low discrimination ratio (**Figure 6L**; two-way mixed ANOVA, Bonferrori adjustment; $F_{1,18}$ = 2.97, p = 0.10; anti-CCK: Familiar 42.63 ± 5.21 s v.s. Novel: 44.87 ± 6.33 s, p = 0.67; anti-scramble: Familiar 34.41 ± 5.30 s v.s. Novel: 49.22 ± 8.87 s, p = 0.01. **Figure 6M**; two sample t-test, df = 18, t = -2.0, anti-CCK: 0.02 ± 0.06 v.s. anti-scramble: 0.19 ± 0.05, p = 0.04), indicating that downregulation of CCK expression in area CA3 was sufficient to impair spatial memory. Taken together, these results support our hypothesis that excitatory CCK acts as a functional neuromodulator in the hippocampal system.

Additionally, for the electrophysiology recording, E-TBS adequately induced LTP at CA3-CA1 synapses in control slices containing the anti-scramble shRNAs, but the same protocol elicited remarkably smaller LTP on slices with anti-CCK shRNA targeting the sequences of CCK gene (**Figures 6N-O**; two way mixed ANOVA, Bonferrori adjustment; $F_{1,14}$ = 10.06, p = 0.007; Pre_{ctrl}: 100.93 ± 0.57 % v.s. $Post_{ctrl}$: 127.78 ± 2.47 %, p < 0.001; Pre_{ex}: 100.44 ± 0.34 % v.s. $Post_{ex}$: 115.76 ±

2.96 %, $p < 0.001$; $Post_{ctrl}$ v.s. $Post_{ex,}$ $p = 0.008$). Moreover, we noticed that the amplitude of the electrically evoked fEPSPs in anti-CCK group is similar to those of the control group (**Figures 6N**, insert), suggesting normal neurotransmission in hippocampal slices from both groups. Therefore, the impairment of LTP is likely due to the reduced expression of CCK in CA1-projecting $CA3^{CCK}$ terminals which impaired the neuromodulation.

Discussion

In the present study, we reported the distribution profile of CCK positive neurons in the dorsal hippocampus, a key brain region associated with spatial memory formation and transformation (Martin and Clark 2007). Although the role of inhibitory CCK neurons is well studied in the hippocampus, the function of excitatory CCK neurons is still unclear. Optogenetic activation of the CCK inhibitory populations produces a prominent IPSC and controls the input and output gain of CA1 pyramidal neurons, and this kind of modulation is mediated by the presynaptic CB1 receptors (Hartzell et al., 2018). A recent study uncovered that systemic activation of CCK-GABA neurons minimally affects emotion but significantly enhances cognition and memory (Whissell et al., 2019). In our study, we combined the Ai14::CCK Cre mice and immunochemistry method to show the distribution of CCK positive neurons in the hippocampus. Moreover, we adopted the pharmacological approach to diminish the tendency for light-evoked fEPSPs of excitatory CA1-projecting $CA3^{CCK}$neurons. Additionally, using the patch clamp technique to record the EPSP of these neurons also can directly validate this conclusion. However, we are unable to conduct whole cell recording due to the limitation of available techniques. To our knowledge, this is the first study that demonstrated the function of excitatory CCK neurons in the hippocampus.

Additionally, to fully validate the involvement of excitatory CA1-projecting $CA3^{CCK}$ neurons in hippocampal processing involving learning and neuroplasticity, we used the chemogenetic technique to examine the function of $CA3^{CCK}$ neurons. Interestingly, we found that specific inhibition of these neurons significantly impaired the CA1-CA3 LTP and attenuated spatial learning. Many studies have also demonstrated that neurotransmitters facilitate the hippocampal plasticity and further modulate the behavior performance (Birthelmer et al., 2003; Ohta et al., 2003; Lopes et al., 2002), because deficiency of neurotransmitters in the CNS is known to be able to decrease the extent of synaptic transmission in the CA3-CA1 pathway. For instance, Mlinar

reported that endogenous 5-hydroxytryptamine (5-HT) potentiates the LTP in the hippocampus and its positive effects on cognitive performance (Mlinar et al., 2015). Also, another study used a viral-mediated approach to delete brain-derived neurotrophic factor (BDNF) specifically in CA3-CA1 pathway, and further demonstrated that presynaptic and postsynaptic BNDF are essential for LTP induction and maintenance, as well as contextual memory impairments (Mohajerani et al., 2007). In this study, we used RNA interference technique (RNAi) to fully characterize the function of $CA3^{CCK}$ neurons. Intriguingly, the knock down of CCK expression significantly impaired LTP formation at excitatory CA1-projecting $CA3^{CCK}$ synapses and further affected the hippocampus dependent-spatial learning and memory. Therefore, we established the essential role of CCK as an active neuromodulator that regulates hippocampal plasticity and its dependent behaviors (**Figure 7**).

Establishing a causal link between neural plasticity and spatial learning is crucial for understanding the status of $CA3^{CCK}$ neurons in the hippocampus. Our investigation verified that $CA3^{CCK}$ neurons modulate hippocampal long-term plasticity in a homosynaptic manner, and their activity underlies spatial learning and memory formation. We demonstrated that the $CA3^{CCK}$ projections to the CA1 region are required and sufficient to induce the LTP at CA3-CA1 synapses. In the behavioral setup, we also observed that the calcium response of CA1-projecting $CA3^{CCK}$ neurons increased during the exploration. The Ca^{2+} activities were also raised throughout the MWM task. Nevertheless, perturbation of the activities of $CA3^{CCK}$ neurons impaired spatial learning both in the NOL task and MWM task. It was likely that the CA3 input to the CA1 conveys spatial information. Thus, we can conclude that $CA3^{CCK}$ neurons may specifically regulate the hippocampal state and plasticity during behavioral performance.

Finally, further experimental works could be undertaken to investigate the function of $CA3^{CCK}$ neurons. For instance, the change of CCK concentration during the light high frequency stimulation of CA1-projecting $CA3^{CCK}$ neurons by using the GPCR-based CCK sensor. Several high-sensitive GPCR-based sensors for detecting the neurotransmitters have been well developed, including the dopamine, norepinephrine, serotonin and acetylcholine. Unfortunately, evidence for CCK release in the hippocampus is not present in this study. Additionally, real time monitoring of CCK release is also critical when animals are subjected to the spatial learning. However, solving

these questions still needs high-sensitive CCK sensor in the future.

Methods

Animals

Adult Cck-IRES-Cre (CCK Cre: RRID:IMSR_JAX:012706) mice and Ai14 mice (RRID:IMSR_JAX:007914) were used in this study. In behavioral experiments, all male mice were housed in a 12-h light/dark cycle and were provided food and water ad libitum. All experimental procedures were approved by the Animal Subjects Ethics Sub-Committee of the City University of Hong Kong.

Viruses

Adeno-associated virus (AAVs) were purchased from the BrainVTA, Wuhan, China: AAV9-CaMKIIa-DIO-GCaMP6S-WPRE-hGH-pA (PT-0090); AAV9-CaMKIIa-DIO-(mCherry-bGH pA-U6)-shRNA(CCK)-WPRE-hGH pA (PT-9086); AAV9-CaMKIIa-DIO-(mCherry-bGH pA-U6)-shRNA(Scramble)-WPRE-hGH pA (PT-3088); AAV9-CaMKIIa-DIO-hM4D(Gi)-mCherry-WPRE-hGH polyA (PT-1143); AAV9-Syn-DIO-mCherry-WPRE-hGH polyA (PT-0115); AAV9-hSyn-CCK sensor 2.3-GFP; AAV9-hSyn-GFP; Addgene, Cambridge, MA, USA: Retrograde AAV-EF1a-DIO-EYFP (27056). Taitool BioScience, Shanghai, China: AAV9-mCaMKIIa-DIO-ChrimsonR-mCherry-ER2-WPRE-pA (S0728-9).

AAV injection

Following deep anesthesia induced by an intraperitoneal injection of pentobarbital sodium (50 mg/kg; Ceva Sante Animale Co., France), each adult mouse was secured in a stereotaxic frame. A midline skin incision exposed the skull, and the stereotaxic apparatus was adjusted to level the skull using the bregma and lambda as landmarks. Using a nanoliter injector (Micro4 system) fitted with a quartz glass micropipette, we delivered the AAV suspension. A small craniotomy was drilled at the predetermined coordinates for the unilateral CA3 region (AP: -1.70 mm, ML: 2.35 mm, DV: -1.85 mm). The AAV was infused at a constant rate of 30 nL/min (volume and titer are specified in the respective figure legends). To prevent backflow, the micropipette remained in

place for 5 minutes post-injection before careful removal. The incision was then sutured and treated with erythromycin ointment to inhibit infection. Mice recovered on a heating pad and were subsequently returned to their housing facility.

Brian slice recording

To prepare for brain slice recording, mice were deeply anesthetized with 1.4% gaseous isoflurane (Wellona Pharma) and decapitated. The brain was rapidly extracted and submerged in ice-cold, oxygenated (95% O_2 / 5% CO_2) artificial cerebrospinal fluid (aCSF) containing (in mM): 124 NaCl, 3 KCl, 1.25 KH_2PO_4, 1.25 $MgSO_4$, 2 $CaCl_2$, 26 $NaHCO_3$, and 10 glucose (pH ~7.4). This same aCSF solution was used for all subsequent steps, including dissection, slicing, incubation, and recording. Coronal sections (300 μm thick) containing the target region were prepared using a vibrating microtome (Leica VT1000S) and were subsequently incubated in aCSF at 32°C for recovery.

For electrophysiological recording, we used a system (Alpha MED Sciences) integrated with a light generator (Inper) to record both electrically- and optically-evoked field excitatory postsynaptic potentials (fEPSPs). Individual hippocampal slices were placed on a multi-electrode array (MEA) probe. One electrode was designated as the stimulating electrode for electrical stimulation. For optical stimulation, a 2-ms pulse of red light (635 nm) was delivered via an optical fiber (200 μm diameter) targeted to the CA1 region. After identifying stable fEPSP responses, input/output (I/O) curves were generated by plotting the fEPSP slope against varying stimulus currents or light intensities. All fEPSP slopes were normalized and analyzed using the MED Mobius software.

Real-time PCR

Tissues of the target brain region (area CA3) were dissected freshly from animals after AAV expression for 4 weeks (AAV carrying anti-CCK or anti-Scramble shRNA). The mRNAs were extracted from the bilateral area CA3 using TRIZOL reagent and reversed transcribed into cDNA with Maxima Reverse Transcriptase (Thermo). CCK gene was then amplified specifically with QuantStudio™ 3 Real-Time PCR System (ABI). The sequences of the primers: CCK-forward, 5’ - AGC GCG ATA CAT CCA GCA G - 3’; CCK-reverse, 5’ - ACG ATG GGT ATT CGT AGT CCT C - 3’. The relative expression level of the CCK gene was analyzed by using the comparative

threshold cycle (C_t) technique (2 -$\Delta\Delta C_t$ method). Three biological replicates were performed and a reference gene (GAPDH) was used to normalize the data of gene expression in this study.

Morris water maze task

Morris water maze (MWM) task follows the Vorhee's protocol (Vorhees and Williams 2006). Briefly, all mice were subjected to the visible platform to access their swimming ability in 122 cm radius swimming pool. Then, during the 5 days training, mice were allowed to locate the hidden platform within 60 seconds which was submerged into the water. The light intensity was set bright enough for the video recording. On day 6, the platform was removed from the target site (quadrant three) of the swimming pool, and all mice were trained to assess the spatial reference memory in the memory retention task. Lastly, the swimming-tracking paths of each mice in different quadrants were analyzed by using the MATLAB software.

Novel object location task

The novel object location (NOL) task was divided into three parts: 10 mins inhabitation for each mouse in the apparatus on day 1, and 5 mins training setup followed by a 5 mins testing setup on day 2. All mice were allowed to interact with two different objects during the training setup, after which animals were transferred into home cage. After 1 hour, mice were subjected to the testing setup in which they were put into the apparatus with the previous two objects, while one object was replaced with a new site. The following formula was carried out to analyze the discrimination index (Pérez-García et al., 2016):

$$\text{Time (NOL)-Time (FOL) / Time (NOL)+Time (FOL)}$$

Note: NOL: novel object location; FOL: familiar object location. A positive/negative value indicates more/less time on exploring the object in a novel location, while zero suggests equal time spent with both objects in familiar and novel locations.

Chemogenetic manipulation

To enable chemogenetic manipulation, CCK-Cre mice were bilaterally implanted with guide cannulas targeting the CA1 hippocampal region (AP: -1.75 mm, ML: ±1.25 mm, DV: -1.20 mm) following viral injection. The surgical protocol was identical to that described previously. Four weeks post-injection, mice underwent hippocampal-dependent memory testing (MWM and NOL

tasks) and electrophysiological assessment. Prior to behavioral tasks, the experimental group (expressing hM4D(Gi)) and the control group (expressing mCherry) received a bilateral microinfusion of Clozapine N-oxide (CNO; 10 μM in 0.1% DMSO) into the CA1 region. Each site received 300 nL at a rate of 50 nL/min via a programmable injector. For in vitro slice recordings, 50 μM CNO was added to the perfusing artificial cerebrospinal fluid (aCSF) during fEPSP recording sessions.

Fiber photometry recording

A fiber-photometry system (Doric Lenses) was employed to record neural activity. The system utilized sinusoidally modulated LEDs (473 nm at 220 Hz and 405 nm at 330 Hz) to excite the GCaMP sensor and capture an isosbestic autofluorescence control signal, respectively. These light signals were conveyed through an implanted optical fiber, with the output intensity calibrated to 10 μW at the fiber tip. Emitted fluorescence was collected via the same fiber and was subsequently focused onto two independent photoreceivers (Newport Corporation, 2151). The entire process-LED control and autonomous demodulation of the 473 nm and 405 nm fluorescence signals-was managed by an RZ5P acquisition system (Tucker-Davis Technologies; TDT) with a built-in real-time processor.

For behavioral correlation, object exploration during the Novel Object Location (NOL) task was defined as the mouse approaching, sniffing, or touching an object. Furthermore, a simplified version of the Morris Water Maze (MWM) task was adapted for compatibility with photometric recordings (Qin et al., 2018). All acquired photometry data were processed using the pMAT open-source software suite (Bruno et al., 2021). The 473 nm signal, representing GCaMP activity, was normalized by fitting the 405 nm isosbestic signal to generate a motion-artifact-corrected $\Delta F/F$ trace according to the standard formula: $\Delta F/F$ = (473 nm signal - fitted 405 nm signal) / fitted 405 nm signal.

Anatomy and histology

All animals were anesthetized with sodium pentobarbital and were perfused with phosphate-buffered saline and fixed with paraformaldehyde solution. Then, mouse's brain was detached and submerged into 4 % PFA solution for fixations at 4 °C in the refrigerator. The brains

were sectioned into 40 mm-thick slices via the vibratome machine. The prepared brain sections were counter-stained with DAPI (1:10000) and mounted onto grass slides with 70% glycerol in PBS to observe the AAV expression and fiber track. Finally, the coverslips were used to cover the brain slices and sealed with adhesive glue.

For the histological procedure, brain slices were washed with 0.01 M PBS and blocked with blocking solution (15 % goat serum mixed with 0.4 % Triton X-100) at room temperature for 2-3 h. Then, the primary antibody was prepared and incubated with brain slices in 24-well cell culture plates overnight at 4 °C. Then, brain slices were washed by 0.01 M PBS and coupled to a secondary antibody at room temperature for 2-3 h. Next, brain slices were washed with PBS and were stained with DAPI. Finally, fluorescence image of brain slices was captured by using a Nikon Eclipse fluorescence microscope and a Nikon A1HD25 confocal microscope.

Statistical analysis

All statistical analyses (including two sample t-test, and two-way mixed ANOVA) were done in SPSS (IBM, USA). Statistical significance was set at $p < 0.05$.

Author contributions: Conceptualization: H.F; Methodology: H.F; Investigation: H.F and A.B; Writing: H.F. and S.T.B.

Conflict of Interest: The authors declare that they have no competing interests.

Acknowledgements: We thank Prof. Jufang He for providing resources. This work was supported by funding from the following: Hong Kong Research Grants Council, General Research Fund: CityUHK 11101521, CityUHK 11103922, CityUHK 11104923, CityUHK 11104524.

Reference

Ali, Afia B (2007) Presynaptic Inhibition of $GABA_A$ Receptor-Mediated Unitary IPSPs by Cannabinoid Receptors at Synapses Between CCK-Positive Interneurons in Rat Hippocampus. *Journal of Neurophysiology* 98(2): 861-69.

Birthelmer, A et al. (2003) Neurotransmitter Release and Its Presynaptic Modulation in the Rat Hippocampus after Selective Damage to Cholinergic or/and Serotonergic Afferents. *Brain Research Bulletin* 59(5): 371-81.

Böhme, Georg Andrees, Jean-Marie Stutzmann, and Jean-Charles Blanchard (1988) Excitatory Effects of Cholecystokinin in Rat Hippocampus: Pharmacological Response Compatible with 'Central'- or B-Type CCK Receptors. *Brain Research* 451(1-2): 309-18.

Broussard, John I. et al. (2016) Dopamine Regulates Aversive Contextual Learning and Associated In Vivo Synaptic Plasticity in the Hippocampus. *Cell Reports* 14(8): 1930-39.

Bruno, Carissa A. et al. (2021) pMAT: An Open-Source Software Suite for the Analysis of Fiber Photometry Data. *Pharmacology Biochemistry and Behavior* 201: 173093.

Cai, Xiang et al. (2013) Local Potentiation of Excitatory Synapses by Serotonin and Its Alteration in Rodent Models of Depression. *Nature Neuroscience* 16(4): 464-72.

Cai, Yuan, and Christopher P. Ford (2018) Dopamine Cells Differentially Regulate Striatal Cholinergic Transmission across Regions through Corelease of Dopamine and Glutamate. *Cell Reports* 25(11): 3148-3157.e3.

Chang, Chin-Chyuan, Ming-Di Hung, and Winton Cheng (2011) Norepinephrine Depresses the Immunity and Disease-Resistance Ability via A1- and B1-Adrenergic Receptors of Macrobrachium Rosenbergii. *Developmental & Comparative Immunology* 35(6): 685-91.

Chen, Lei et al. (2021) Cholecystokinin Octapeptide Improves Hippocampal Glutamatergic Synaptogenesis and Postoperative Cognition by Inhibiting Induction of A1 Reactive Astrocytes in Aged Mice. *CNS Neuroscience & Therapeutics* 27(11): 1374-84.

Chowdhury, Rumana et al. (2012) Dopamine Modulates Episodic Memory Persistence in Old Age. *The Journal of Neuroscience* 32(41): 14193-204.

De Wied, D (1997) Neuropeptides in Learning and Memory Processes. *Behavioural Brain Research* 83(1-2): 83-90.

Ge, Yuan et al. (2010) Hippocampal Long-Term Depression Is Required for the Consolidation of Spatial Memory. *Proceedings of the National Academy of Sciences* 107(38): 16697-702.

Gedankien, Tamara et al. (2023) Acetylcholine Modulates the Temporal Dynamics of Human Theta Oscillations during Memory. *Nature Communications* 14(1): 5283.

Gomez, Juan L. et al. (2017) Chemogenetics Revealed: DREADD Occupancy and Activation via Converted Clozapine. *Science* 357(6350): 503-7.

Goodman, Anthoni M. et al. (2021) Heightened Hippocampal β-Adrenergic Receptor Function Drives Synaptic Potentiation and Supports Learning and Memory in the TgF344-AD Rat Model during Prodromal Alzheimer's Disease. *The Journal of Neuroscience* 41(26): 5747-61.

Grasselli, Giorgio, and Christian Hansel (2014). Cerebellar Long-Term Potentiation. In *International Review of Neurobiology*, Elsevier, 39-51.

Hamilton, Trevor J. et al. (2010) Dopamine Modulates Synaptic Plasticity in Dendrites of Rat and Human Dentate Granule Cells. *Proceedings of the National Academy of Sciences* 107(42): 18185-90.

Hartzell, Andrea L et al. (2018) NPAS4 Recruits CCK Basket Cell Synapses and Enhances Cannabinoid-Sensitive Inhibition in the Mouse Hippocampus. *eLife* 7: e35927.

Hefft, Stefan, and Peter Jonas (2005) Asynchronous GABA Release Generates Long-Lasting Inhibition at a

Hippocampal Interneuron-Principal Neuron Synapse. *Nature Neuroscience* 8(10): 1319-28.

Karayol, Remzi et al. (2021) Serotonin Receptor 4 in the Hippocampus Modulates Mood and Anxiety. *Molecular Psychiatry* 26(6): 2334-49.

Kempadoo, Kimberly A. et al. (2016) Dopamine Release from the Locus Coeruleus to the Dorsal Hippocampus Promotes Spatial Learning and Memory. *Proceedings of the National Academy of Sciences* 113(51): 14835-40.

Klausberger, Thomas et al. (2005) Complementary Roles of Cholecystokinin- and Parvalbumin-Expressing GABAergic Neurons in Hippocampal Network Oscillations. *The Journal of Neuroscience* 25(42): 9782-93.

Lopes, L.V. et al. (2002) Adenosine A2A Receptor Facilitation of Hippocampal Synaptic Transmission Is Dependent on Tonic A1 Receptor Inhibition. *Neuroscience* 112(2): 319-29.

Ma, Yihe, and William J. Giardino (2022) Neural Circuit Mechanisms of the Cholecystokinin (CCK) Neuropeptide System in Addiction. *Addiction Neuroscience* 3: 100024.

Martin, S. J., and R. E. Clark (2007) The Rodent Hippocampus and Spatial Memory: From Synapses to Systems. *Cellular and Molecular Life Sciences* 64(4): 401-31.

Merighi, Adalberto, Chiara Salio, Francesco Ferrini, and Laura Lossi (2011) Neuromodulatory Function of Neuropeptides in the Normal CNS. *Journal of Chemical Neuroanatomy* 42(4): 276-87.

Mineur, Yann S. et al. (2013) Cholinergic Signaling in the Hippocampus Regulates Social Stress Resilience and Anxiety- and Depression-like Behavior. *Proceedings of the National Academy of Sciences* 110(9): 3573-78.

Mlinar, Boris, Gabriella Stocca, and Renato Corradetti (2015) Endogenous Serotonin Facilitates Hippocampal Long-Term Potentiation at CA3/CA1 Synapses. *Journal of Neural Transmission* 122(2): 177-85.

Mohajerani, Majid H. et al. (2007) Correlated Network Activity Enhances Synaptic Efficacy via BDNF and the ERK Pathway at Immature CA3-CA1 Connections in the Hippocampus. *Proceedings of the National Academy of Sciences* 104(32): 13176-81.

Nakamura, N.H., K. Akiyama, and T. Naito (2011) Suppression of cAMP-Dependent Gene Expression by Cholecystokinin in the Hippocampus. *Neuroscience* 187: 15-23.

Nishimura, Sayoko et al. (2015) Functional Synergy between Cholecystokinin Receptors CCKAR and CCKBR in Mammalian Brain Development. *PLOS ONE* 10(4): e0124295.

Ohta, Kohei et al. (2003) Stearic Acid Facilitates Hippocampal Neurotransmission by Enhancing Nicotinic ACh Receptor Responses via a PKC Pathway. *Molecular Brain Research* 119(1): 83-89.

Park, Hyungju, Andrei Popescu, and Mu-ming Poo (2014) Essential Role of Presynaptic NMDA Receptors in Activity-Dependent BDNF Secretion and Corticostriatal LTP. *Neuron* 84(5): 1009-22.

Pérez-García, Georgina, Omar Guzmán-Quevedo, Raquel Da Silva Aragão, Francisco Bolaños-Jiménez (2016). Early Malnutrition Results in Long-Lasting Impairments in Pattern-Separation for Overlapping Novel Object and Novel Location Memories and Reduced Hippocampal Neurogenesis. *Scientific Reports* 6(1): 21275.

Picciotto, Marina R., Michael J. Higley, and Yann S. Mineur (2012) Acetylcholine as a Neuromodulator: Cholinergic Signaling Shapes Nervous System Function and Behavior. *Neuron* 76(1): 116-29.

Qin, Han et al. (2018) A Visual-Cue-Dependent Memory Circuit for Place Navigation. *Neuron* 99(1): 47-55. e4.

Ranganath, Charan, and Liang-Tien Hsieh (2016) The Hippocampus: A Special Place for Time: The Hippocampus: A Special Place for Time. *Annals of the New York Academy of Sciences* 1369(1): 93-110.

Reisi, Parham et al. (2015) Effect of Cholecystokinin on Learning and Memory, Neuronal Proliferation and Apoptosis in the Rat Hippocampus. *Advanced Biomedical Research* 4(1): 227.

Swaab, D.F (1982) Neuropeptides. Their Distribution and Function in the Brain." In *Progress in Brain Research*, Elsevier, 97-122.

Takács, Virág T. et al. (2018) Co-Transmission of Acetylcholine and GABA Regulates Hippocampal States. *Nature Communications* 9(1): 2848.

Vorhees, Charles V, and Michael T Williams (2006) Morris Water Maze: Procedures for Assessing Spatial and Related Forms of Learning and Memory. *Nature Protocols* 1(2): 848-58.

Wei, Xiao-fei et al. (2013). CCK-8S Increases the Firing Frequency of CCK-Positive Neurons and Facilitates Excitatory Synaptic Transmission in Primary Rat Hippocampal Neurons. *Neuroscience Letters* 549: 34-39.

Wen, Di et al. (2014) Cholecystokinin-Octapeptide Restored Morphine-Induced Hippocampal Long-Term Potentiation Impairment in Rats. *Neuroscience Letters* 559: 76-81.

Whissell, Paul D. et al. (2019) Selective Activation of Cholecystokinin-Expressing GABA (CCK-GABA) Neurons Enhances Memory and Cognition. *eneuro* 6(1): ENEURO.0360-18.2019.

Xing, Bo, Yan-Chun Li, Wen-Jun Gao (2016) Norepinephrine versus Dopamine and Their Interaction in Modulating Synaptic Function in the Prefrontal Cortex. *Brain Research* 1641: 217-33.

Zakharenko, Stanislav S et al. (2003) Presynaptic BDNF Required for a Presynaptic but Not Postsynaptic Component of LTP at Hippocampal CA1-CA3 Synapses. *Neuron* 39(6): 975-90.

Figure Legends

Figure 1. The distribution profile of CCK-positive neurons in the dorsal hippocampus.

(A) Schematic flowchart of mating strategy to obtain CCK Cre/Ai14 mice.

(B) Fluorescence image of the dorsal hippocampus slice of CCK Cre/Ai14 stained with neuron marker (NeuN, rabbit anti-488). Scale bar: 1000 μm.

(C) CCK positive neurons were double labelled by tdTomato (Red) and rabbit anti-488 (GFP) in the area CA1 and CA3. Scale bar: 50 μm.

(D) Quantification of CCK+ neurons in the CA1 area and CA3 area.

(E) Example of co-immunofluorescent staining of CCK positive neurons with excitatory neuronal marker (CamKIIα) in CA3 area. Scale bar: 100 μm.

(F) Fluorescence image of the colocalization between CCK protein (Pro-CCK) and excitatory marker in CA3 area. Scale bar: 1000 μm.

(G) Schematic diagram of virus injection. AAV-EF1α-DIO-EYFP (6.5 E+12 vg/ml, 50 nl) was injected into CA1 area of CCK Cre mice.

(H) Representative image of AAV injection in the hippocampal CA1 (left, scale bar: 1000 μM). Detailed view of retrogradely labeled neurons in area CA3 (right, scale bar: 100 μm).

(I) Representative image showing the colocalization between the Cre-dependent retro AAV (gfp) and CamKIIα (rabbit anti-589: red). Scale bar: 100 μm.

(J) Co-immunofluorescent staining of GFP with the excitatory neuronal marker CamKIIα in area CA3 of CCK Cre mice.

Figure 2. Excitatory CA3 neurons secret the neuropeptide CCK.

(A) Schematic diagram of virus injection. AAV9-DIO-CamKIIα-mCherry (5.0 E+12 vg/ml, 250 nl) was injected into CA3 area of CCK Cre mice.

(B) Viral expression in the hippocampal CA3 area and its projections in the CA1 area, scale bar: 1000 μm.

(C) A magnified view of the square area (1; scale bar, 50 μm).

(D) Schematic drawing of the brain slice recording in the hippocampus.

(E) Representative L-fEPSP of CCK+ SC projections by light stimulation before and after application of CNQX+ APV. Scale, 0.2 mV by 10 msec.

(F) Quantitative analysis of the glutamatergic transmission in $CA3^{CCK}$-CA1 projections.

(G) Schematic showing the neurological principle of the CCK sensor. CCK ligand binds the sensor and induces a change in fluorescence of CCK sensor.

(H) Schematic diagram showing injection of AAV9-hSyn-CCK sensor 2.3 (5.75E + 12 vg/ ml, 200 nl) and AAV9-CamKIIα-DIO-ChrimsonR-mCherry (5.0 E + 12 vg/ ml, 250 nl) into the CA3 and CA1 area. followed by laser stimulation and photometry recording.

(I) CCK sensor expression in the CA1 area around fiber tip, scale bar: 1000 μm, and ChrimsonR expressing CA3-CA1 projectionsof CCK-Cre mice.

(J) Magnified images showing the stimulation site and recording site.

(K) Hypothetical model depicting the neuronal activity-dependent CCK release from CA3 pre-synapse in the CA1 area.

(L) The heatmap results showing the Ca^{2+} response in each mice after the L-TBS in GFP group (upper; N= 3, n = 6 trials) and CCK-sensor group (lower; N= 3, n = 6 trials).

(M) Averaged fluorescence increases in response to optogenetic stimulation (635 nm L-TBS; $N = 3$ animals, $n = 6$ trials for each group).

(N) Quantification of averaged fluorescence in the CCK-Cre mice (averaged the Δ F/F after L-TBS within 3 s).

$^{*}p < 0.05$, $^{**}p < 0.01$, $^{***}p < 0.001$; ns not significant. Data are reported as mean ± SEM.

Figure 3. $CA3^{CCK}$ neurons fire actively during hippocampal-dependent tasks

(A) Schema of the novel location task and Morris water maze task.

(B) Viral injection location in the CA3 area, and labeled CCK positive neurons in the CA3 of the CCK Cre mice. AAV9-CaMKIIa-DIO-GCaMP6s (5.00E+12 vg/ ml, 300 nl); Scale bar: 1000 μm and 100 μm.

(C) The mice displayed significantly more interactions with the novel placed object than with the familiar object.

(D) Heatmap shows the Δ *F/F* average traces from a single subject in the training and testing phase. N= 6 mice.

(E) The Δ *F/F* average traces from all subject animals (N = 6), aligned to the time of object interaction.

(F) Mean GCaMP6s signals of the $CA3^{CCK}$ neurons during bouts of object exploration in training and testing trials (average 1.5 seconds data after the indicated events).

(G) Schematic drawing depicts the experimental setup for Ca^{2+} recording during the MWM task.

(H) Plot of the Δ *F/F* (black) and their corresponding escape latencies (red) during the MWM task.

(I) Heatmap and mean GCaMP6s signals of the original-trained state (trial 1).

(J) Heatmap and mean GCaMP6s signals of the well-trained state (trial 9).

(K) Summary of the Δ *F/F* between the trial 1 and trial 9 (average 10 seconds data after the indicated events).

$^{*}p < 0.05$, $^{**}p < 0.01$, $^{***}p < 0.001$; ns, not significant. Data are reported as mean ± SEM.

Figure 4. Chemogenetic inhibition of the excitatory $CA3^{CCK}$-CA1 pathway impairs behavioral tasks.

(A) Schematic of Cre-dependent color-switch labeling in the CA3-CA1 projections of CCK-Cre mice (AAV9-CaMKIIa-DIO-hM4D(Gi)-mCherry, 6.50 + 12 vg/mL, 300 nl; AAV9-hSyn-DIO-mCherry, 6.50 + 12 vg/mL; 300 nl).

(B) Viral expression with the cannula track in the area CA1, scale bar, 1,000 μm. Magnified image is shown on the right (scale bar, 100 μm).

(C) Schematic of the Morris water maze (MWM) task. The hidden platform is placed in the southwestern (SW) site (quadrant 3).

(D) Quantitative data analysis for swimming speed of two groups of mice in locating the platform during the visible platform task.

(E) Quantitative data analysis for swimming time of two groups of mice in locating the platform during the visible platform task.

(F) Escape latency of two groups of mice during training phases of the MWM.

(G) Swimming traces of two groups of mice in the spatial probe trial of memory retention test.

(H) The proportion of total time of two groups of mice spent in each quadrant.

(I) Protocol of the novel object location task. Details is depicted in the method section.

(J) The total exploration time for either object shows no significant statistical difference.

(K) Controls (Only expressing mCherry) exhibited obviously more interactions with the novel placed object than with the familiar object compared to the HM4D(Gi) group.

(L) HM4D(Gi) group scored significantly less on the discrimination ratio compared to controls.

$^{*}p < 0.05$, $^{**}p < 0.01$, $^{***}p < 0.001$; ns, not significant. Data are reported as mean ± SEM.

Figure 5. Chemogenetic inhibition of the excitatory $CA3^{CCK}$-CA1 pathway impairs LTP formation.

(A) Schematic diagram of virus injection. AAV9-CaMKIIa-DIO-hM4D(Gi)-mCherry (5.0 E+12 vg/ml, 300 nl) or AAV9-Syn-DIO-mCherry (5.0 E+12 vg/ml, 300 nl) was injected into CA3 area of CCK Cre mice.

(B) Left: viral expression in the hippocampal CA3 area and its projections in the CA1 area, scale bar: 1000 μM; Right: a magnified view of the square area (1; scale bar, 100 μm).

(C) Schematic drawing of the brain slice recording in the hippocampus.

(D) CNO infusion caused a remarkable decline in E-fEPSP from the HM4D(Gi) expressing slices compared to controls (mCherry). Scale, 0.2 mV by 10 msec.

(E) Quantitative data analysis for the E-fEPSP between the experimental group and controls.

(F) The protocol of electrical theta burst stimulation (E-TBS) for eliciting LTP.

(G) LTP was attenuated in the HM4D(Gi) expressing slices compared to controls (mCherry). Scale, 0.2 mV by 10 ms.

(H) Quantitative data analysis for the E-fEPSP between the experimental group and controls.

$^{*}p < 0.05$, $^{**}p < 0.01$, $^{***}p < 0.001$; ns, not significant. Data are reported as mean ± SEM.

Figure 6. RNA interference of excitatory $CA3^{CCK}$ expression attenuates hippocampal functions.

(A) Schematic diagram of virus injection. AAV9-CaMKIIa-DIO-(mCherry-bGH pA-U6)-shRNA-CCK (5.0 E+12 vg/ml, 300 nl) or AAV9-CaMKIIa-DIO-(mCherry-bGH pA-U6)-shRNA-Scramble (5.0 E+12 vg/ml, 300 nl) was injected into area CA3 of CCK Cre mice.

(B) Left: viral expression in the hippocampal CA3 and its projections in the CA1 area, scale bar: 1000 μM; Right: a magnified view of the square area (1; scale bar, 100 μm).

(C) Quantification of the CCK mRNA expression in the CA3 of CCK Cre mice that infected with anti-CCK or anti-scramble shRNA.

(D) Schematic drawing of the brain slice recording in the hippocampus.

(E) Quantitative data analysis for swimming speed of two groups of mice in locating the platform during the visible platform task.

(F) Quantitative data analysis for swimming time of two groups of mice in locating the platform during the visible platform task.

(G) Escape latency of two groups of mice during training phases of the MWM.

(H) Swimming traces of two groups of mice in the spatial probe trial of memory retention test.

(I) The proportion of total time of two groups of mice spent in each quadrant.

(J) Protocol of the novel object location task. Details is depicted in the method section.

(K) The total exploration time for either object shows no significant statistical difference.

(L) Controls (anti-scramble) exhibited obviously more interactions with the novel placed object than with the familiar object compared to the anti-CCK group.

(M) Anti-CCK group scored significantly less on the discrimination ratio compared to the anti-scramble group.

(N) LTP was attenuated in the anti-CCK expressing slices compared to controls (anti-scramble). Scale, 0.2 mV by 10 ms.

(O) Quantitative data analysis for the E-fEPSP between the experimental group and controls.

$^{*}p < 0.05$, $^{**}p < 0.01$, $^{***}p < 0.001$; ns, not significant. Data are reported as mean ± SEM.

Figure 7. Summary of the neural effects

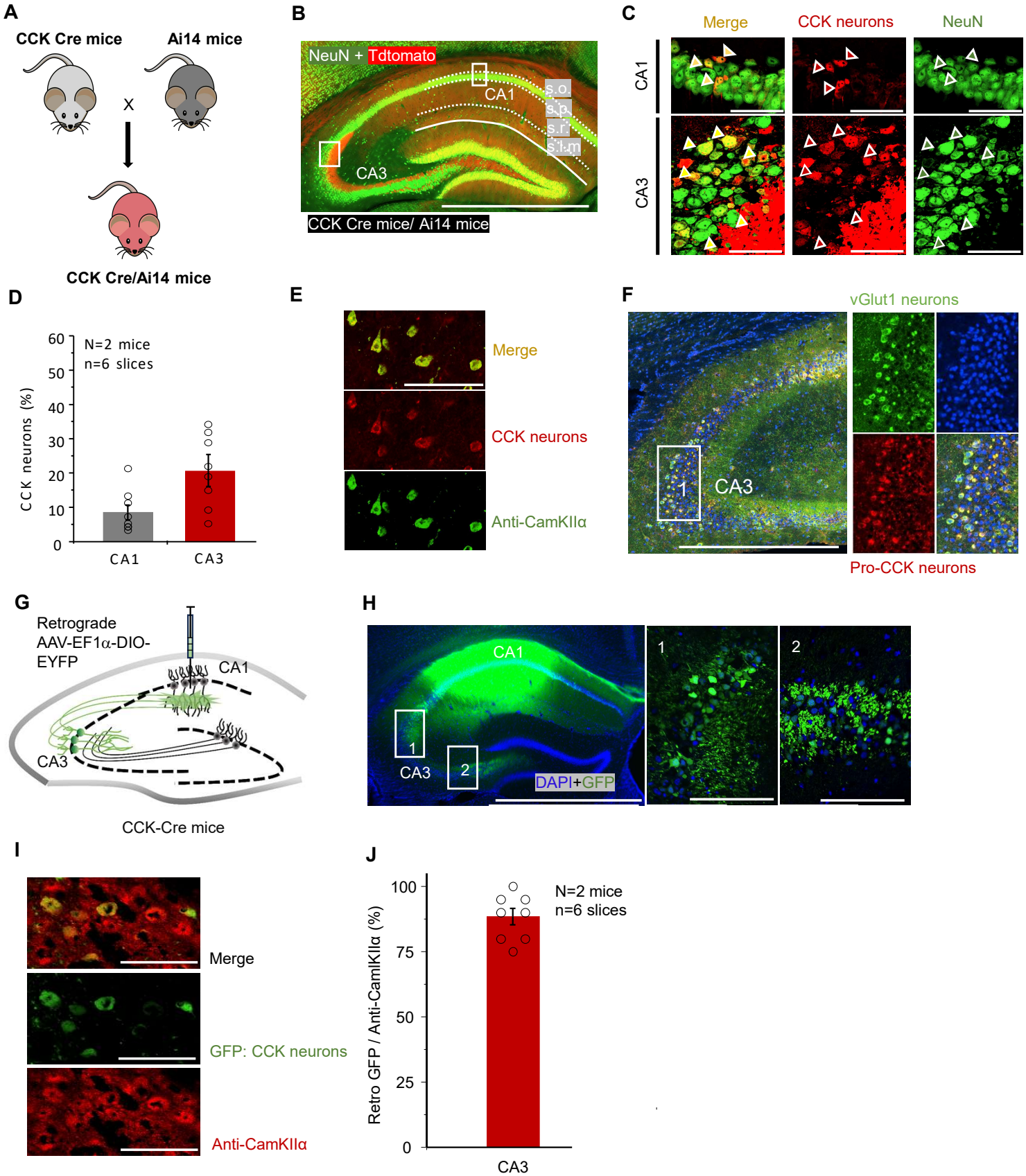
A
CCK Cre mice
Ai14 mice
X
CCK Cre/Ai14 mice
B
NeuN + Tdtomato
CA1
CA3
s.o.
s.p.
s.r.
s.l.m
CCK Cre mice/ Ai14 mice
C
Merge
CCK neurons
NeuN
CA1
CA3
D
N=2 mice
n=6 slices
CCK neurons (%)
60
50
40
30
20
10
0
CA1
CA3
E
Merge
CCK neurons
Anti-CamKIIα
F
vGlut1 neurons
1
CA3
Pro-CCK neurons
G
Retrograde
AAV-EF1α-DIO-
EYFP
CA1
CA3
CCK-Cre mice
H
CA1
1
CA3
2
DAPI+GFP
1
2
I
Merge
GFP: CCK neurons
Anti-CamKIIα
J
N=2 mice
n=6 slices
Retro GFP / Anti-CamKIIα (%)
100
75
50
25
0
CA3

Figure 1

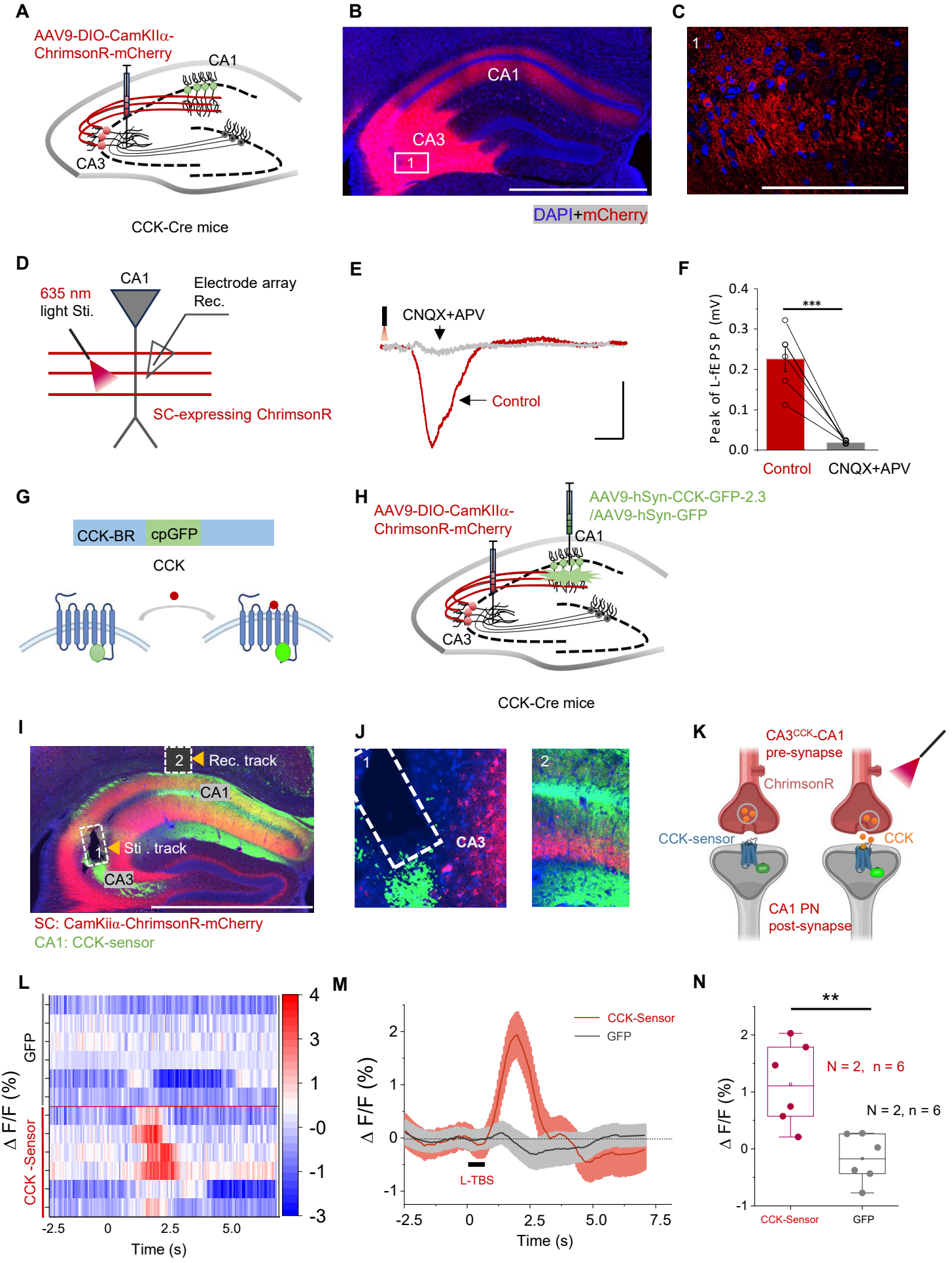
A
AAV9-DIO-CamKIIα-ChrimsonR-mCherry
CA1
CA3
CCK-Cre mice
B
CA1
CA3
1
DAPI+mCherry
C
1
D
CA1
635 nm light Sti.
Electrode array Rec.
SC-expressing ChrimsonR
E
CNQX+APV
Control
F
Peak of L-fEPSP (mV)
0.4
0.3
0.2
0.1
0.0
***
Control
CNQX+APV
G
CCK-BR
cpGFP
CCK
H
AAV9-DIO-CamKIIα-ChrimsonR-mCherry
AAV9-hSyn-CCK-GFP-2.3 /AAV9-hSyn-GFP
CA1
CA3
CCK-Cre mice
I
2
Rec. track
CA1
1
Sti . track
CA3
SC: CamKiiα-ChrimsonR-mCherry
CA1: CCK-sensor
J
1
CA3
2
K
CA3CCK-CA1 pre-synapse
ChrimsonR
CCK-sensor
CCK
CA1 PN post-synapse
L
GFP
CCK -Sensor
Δ F/F (%)
4
3
1
-0
-1
-3
-2.5
0
2.5
5.0
Time (s)
M
CCK-Sensor
GFP
Δ F/F (%)
2
1
0
-1
L-TBS
-2.5
0
2.5
5.0
7.5
Time (s)
N
**
N = 2, n = 6
N = 2, n = 6
Δ F/F (%)
2
1
0
-1
CCK-Sensor
GFP

Figure 2

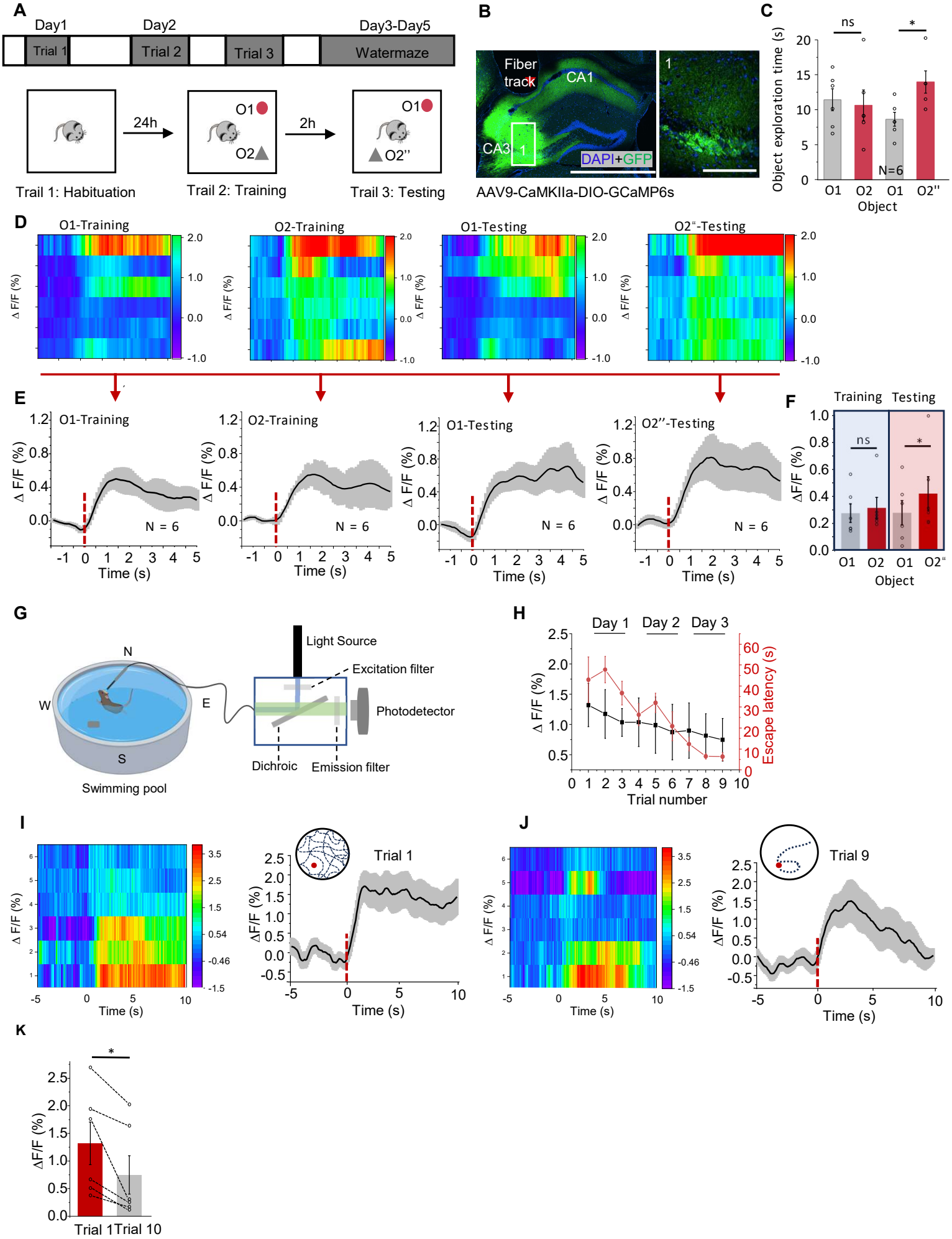
A
Day1
Day2
Day3-Day5
Trial 1
Trial 2
Trial 3
Watermaze
24h
2h
O1
O2
O2''
Trail 1: Habituation
Trail 2: Training
Trail 3: Testing
B
Fiber track
CA1
CA3
DAPI+GFP
AAV9-CaMKIIa-DIO-GCaMP6s
C
ns
*
Object exploration time (s)
N=6
O1
O2
O1
O2''
Object
D
O1-Training
O2-Training
O1-Testing
O2''-Testing
Δ F/F (%)
E
O1-Training
O2-Training
O1-Testing
O2''-Testing
N = 6
Time (s)
F
Training
Testing
ns
*
Object
G
N
W
E
S
Swimming pool
Light Source
Excitation filter
Photodetector
Dichroic
Emission filter
H
Day 1
Day 2
Day 3
Escape latency (s)
Trial number
I
Trial 1
Time (s)
J
Trial 9
Time (s)
K
*
Trial 1
Trial 10

Figure 3

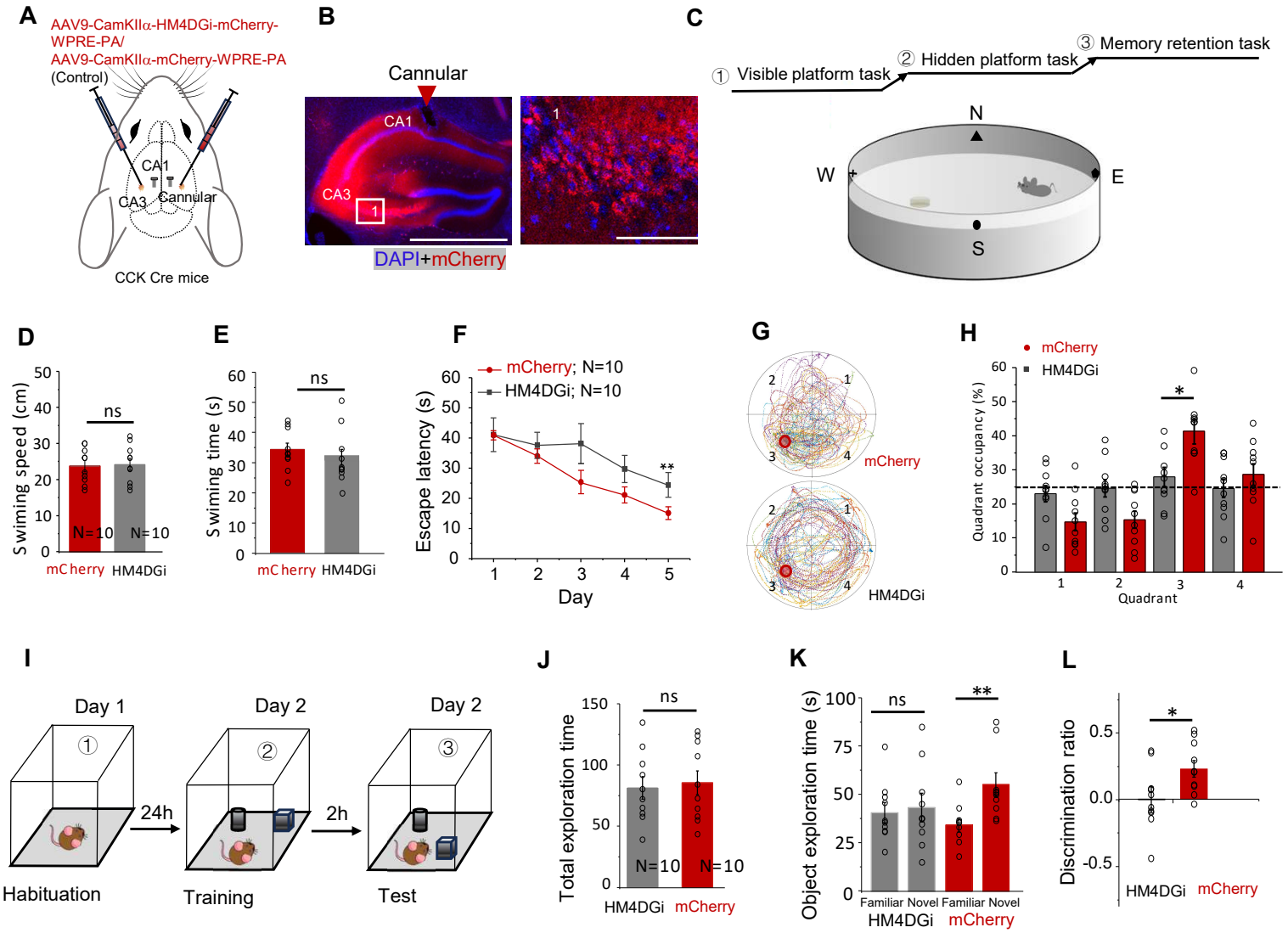
A
AAV9-CamKIIα-HM4DGi-mCherry-WPRE-PA/
AAV9-CamKIIα-mCherry-WPRE-PA
(Control)
CA1
CA3
Cannular
CCK Cre mice
B
Cannular
CA1
CA3
1
DAPI+mCherry
C
① Visible platform task
② Hidden platform task
③ Memory retention task
N
W
E
S
D
Swiming speed (cm)
ns
N=10
N=10
mCherry
HM4DGi
E
Swiming time (s)
ns
mCherry
HM4DGi
F
Escape latency (s)
mCherry; N=10
HM4DGi; N=10
**
Day
G
mCherry
HM4DGi
H
mCherry
HM4DGi
Quadrant occupancy (%)
*
Quadrant
I
Day 1
Day 2
Day 2
24h
2h
Habituation
Training
Test
J
Total exploration time
ns
N=10
N=10
HM4DGi
mCherry
K
Object exploration time (s)
ns
**
Familiar Novel Familiar Novel
HM4DGi
mCherry
L
Discrimination ratio
*
HM4DGi
mCherry

Figure 4

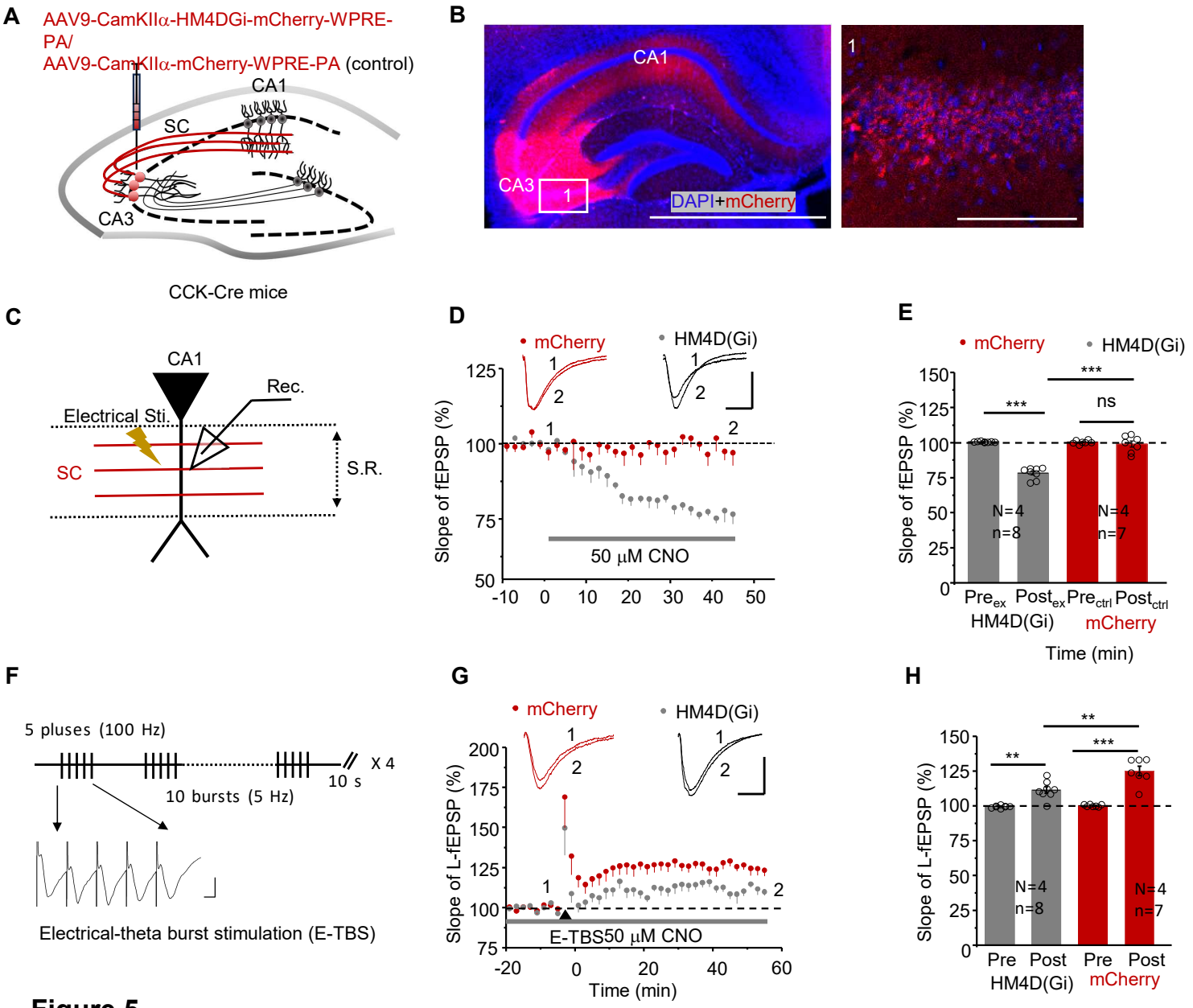
A
AAV9-CamKIIα-HM4DGi-mCherry-WPRE-PA/
AAV9-CamKIIα-mCherry-WPRE-PA (control)
CA1
SC
CA3
CCK-Cre mice
B
CA1
CA3
1
DAPI+mCherry
C
CA1
Rec.
Electrical Sti.
SC
S.R.
D
mCherry
HM4D(Gi)
Slope of fEPSP (%)
50 μM CNO
E
mCherry
HM4D(Gi)
Slope of fEPSP (%)
***
ns
N=4
n=8
N=4
n=7
Pre_ex Post_ex Pre_ctrl Post_ctrl
HM4D(Gi)
mCherry
Time (min)
F
5 pluses (100 Hz)
X 4
10 s
10 bursts (5 Hz)
Electrical-theta burst stimulation (E-TBS)
G
mCherry
HM4D(Gi)
Slope of L-fEPSP (%)
E-TBS50 μM CNO
Time (min)
H
Slope of L-fEPSP (%)
**
***
N=4
n=8
N=4
n=7
Pre Post Pre Post
HM4D(Gi)
mCherry

Figure 5

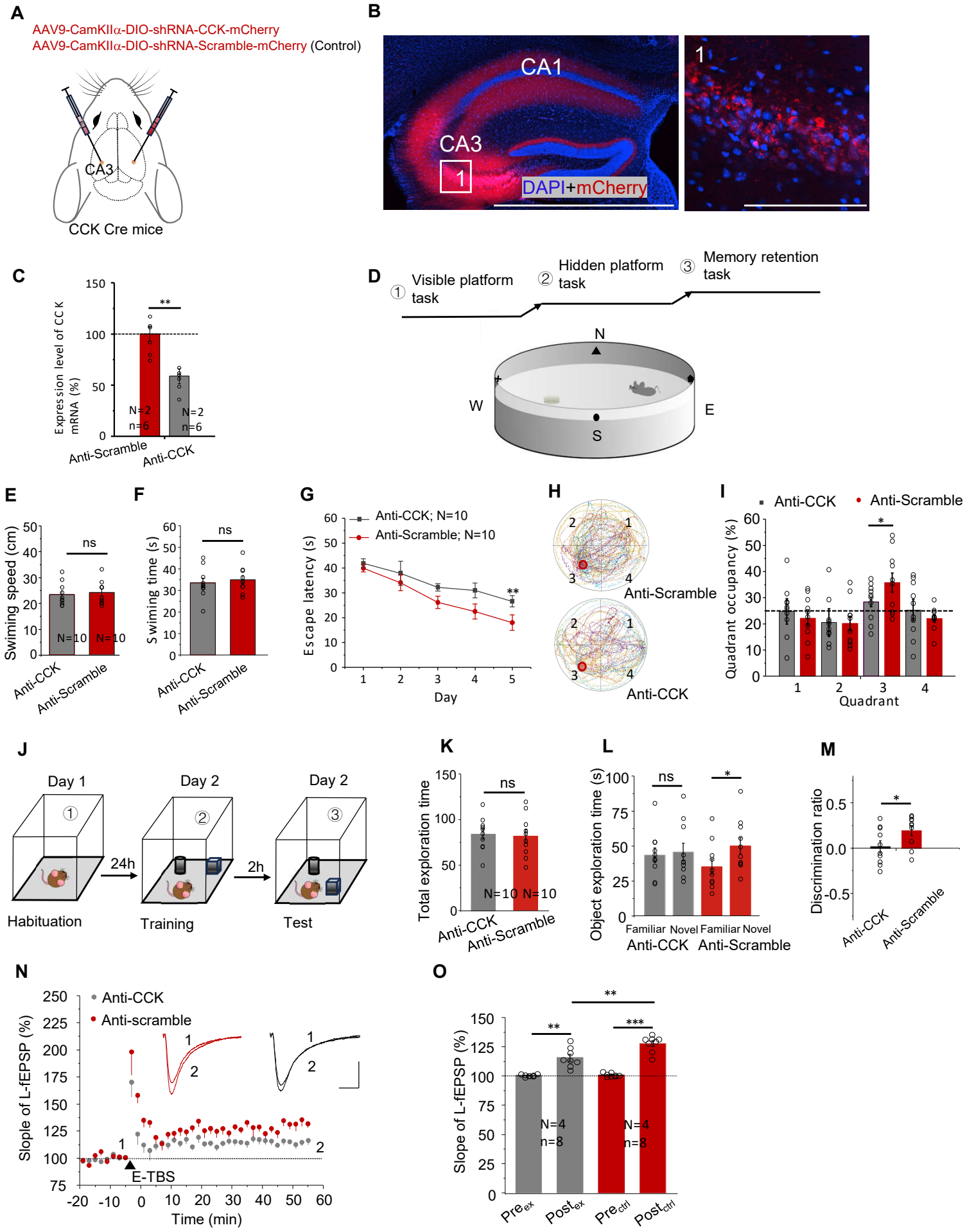
A
AAV9-CamKIIα-DIO-shRNA-CCK-mCherry
AAV9-CamKIIα-DIO-shRNA-Scramble-mCherry (Control)
CA3
CCK Cre mice
B
CA1
CA3
1
DAPI+mCherry
1
C
Expression level of CCK mRNA (%)
150
100
50
0
**
N=2
n=6
N=2
n=6
Anti-Scramble
Anti-CCK
D
① Visible platform task
② Hidden platform task
③ Memory retention task
N
W
E
S
E
Swiming speed (cm)
ns
N=10
N=10
Anti-CCK
Anti-Scramble
F
Swiming time (s)
ns
Anti-CCK
Anti-Scramble
G
Escape latency (s)
Anti-CCK; N=10
Anti-Scramble; N=10
**
Day
H
Anti-Scramble
Anti-CCK
I
Anti-CCK
Anti-Scramble
Quadrant occupancy (%)
*
Quadrant
J
Day 1
Day 2
Day 2
24h
2h
Habituation
Training
Test
K
Total exploration time
ns
N=10
N=10
Anti-CCK
Anti-Scramble
L
Object exploration time (s)
ns
*
Familiar
Novel
Familiar
Novel
Anti-CCK
Anti-Scramble
M
Discrimination ratio
*
Anti-CCK
Anti-Scramble
N
Slope of L-fEPSP (%)
Anti-CCK
Anti-scramble
E-TBS
Time (min)
O
Slope of L-fEPSP (%)
**
**
***
N=4
n=8
N=4
n=8
Pre_ex
Post_ex
Pre_ctrl
Post_ctrl

Figure 6

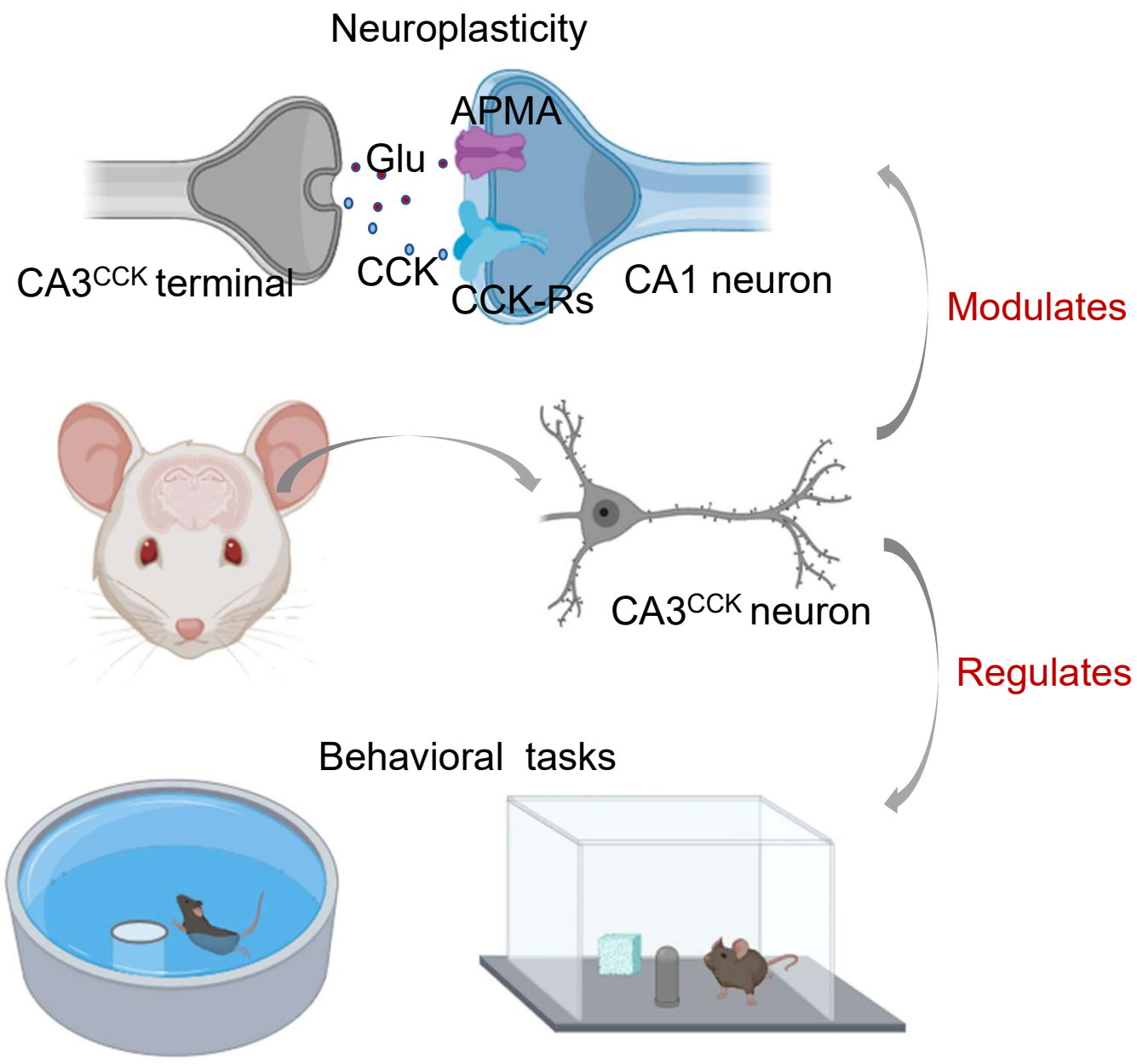
Neuroplasticity
APMA
Glu
CCK
CCK-Rs
CA3CCK terminal
CA1 neuron
Modulates
CA3CCK neuron
Regulates
Behavioral tasks

Figure 7